Journal of Earthquake Engineering,
Vol. 8, Special Issue 1 (2004) 187–224

Imperial College Press
www.icpress.co.uk

EFFECTS OF AXIAL FORCE VARIATION IN THE SEISMIC RESPONSE OF BRIDGES ISOLATED WITH FRICTION PENDULUM SYSTEMS

G. M. CALVI, P. CERESA and C. CASAROTTI

European School for Advanced Studies in Reduction of Seismic Risk (ROSE School), Via Ferrata 17, 27100 Pavia, Italy

D. BOLOGNINI

European Centre for Training and Research in Earthquake Engineering, Via Ferrata, 1, 27100, Pavia, Italy

F. AURICCHIO

Dipartimento di Meccanica Strutturale, Università degli Studi di Pavia, Via Ferrata 1, 27100 Pavia, Italy

The effects of the axial load variations on the seismic response of bridges isolated with friction pendulum systems (FPS) are investigated. A series of parametric time history non-linear analyses are performed for different bridge configurations, defined after an extensive investigation on typical existing cases. The influence of both horizontal and vertical components of the ground motion is considered. The behaviour of the pier-isolator-deck system is predicted using two analytical models characterised by hysteretic loops sensitive or insensitive to axial force variations, in order to compare the different responses. Level of axial force, maximum displacements and induced bending moment are investigated, as well as shear and torsion demand, caused by different shear actions acting on the isolator devices. A comparison between demand and resistance capacity of the bridge piers is performed, in order to investigate possible non-conservative approaches in the current design methods and to raise controversial issues on the subject.

Keywords: Friction pendulum system; isolated bridges; axial force variation; shear demand; seismic response.

1. Foreword

The importance of the vertical seismic input in the structural response of bridges has been investigated by various authors [Ambraseys and Douglas, 2000; Ghobarah and Elnashai, 1998; Elnashai and Papazoglou, 1997]. The damaging effects of the vertical component of an earthquake are more evident in the near field since the vertical motion attenuates faster than the horizontal one; in this case ground motions from large earthquakes ($M_s > 7$) can produce significant horizontal and vertical components and the ratio of the vertical to horizontal maximum PGA may exceed 1.

The energy content of the vertical component is concentrated in a narrow high frequency range. This results in a possibly dangerous match with the vertical periods of common bridges, usually belonging to the higher frequency range. Furthermore, several records indicate that the maximum vertical response occurs 1 or 2 seconds earlier than the transverse one, others show a coincidence in time. A compendium of field observations and analytical results indicates that certain failure modes are convincingly attributable to high vertical earthquake-induced forces, which, in addition to the possible overstressing in compression or tension, may induce shear or flexure failure.

In bridges, a reduction of earthquake effects is often obtained using seismic isolation techniques. The actual technologies include various types of rubber and sliding bearings, in particular the friction pendulum systems (FPS), which have found several applications in the recent years, will be examined in this research. A standard FPS device is based on the well-known principles of the sliding pendulum. Its main peculiarities are the re-centring capacity (in terms of restoring forces by gravity) and the use of geometry and gravity to achieve the desired isolated response of the structures.

Since friction pendulum systems may be strongly influenced by the axial load level acting at a given time, a variation of the axial force results in corresponding variations of equivalent yielding level and in the post-yielding stiffness in the non-linear phase of the hysteretic response. Numerical models insensitive to axial force variations may not appropriately predict the real response of isolated bridges. In particular these models do not take into account possible increments in the shear force demand and potential torsional effects on the piers. The axial force variation on an isolation device is not only affected by the vertical acceleration, but also depends on a combination of effects due to horizontal input (because of the necessary dynamic equilibrium to the horizontal forces) and to the geometrical configuration (plan and elevation irregularities).

In this study, a first contribution to the definition of the relevant aspects of the problem is presented, based on a large number of dynamic analyses of two fundamental bridge configurations (straight and curved bridges with piers of the same height of 10 m and 30 m).

2. Objectives

The objectives of the research presented in this paper are:

- To develop and test an analytical model of FPS, that takes into account the effect of axial force variations on the isolators. Existing formulations and analytical models are based on bilinear hysteretic loops with constant yielding shear value and constant post-yielding hardening, while yielding shear value and post-elastic stiffness of FPS depend on acting axial force, resulting in hysteretic loops characterised by non-linear post-elastic branch.

- To explore the geometrical parameters of typical deck cross sections that define cases sensitive to axial force variation, for which the prediction of the overall response of the structure is particularly influenced by the characteristics of the model.
- To perform systematic evaluation of the axial load and shear actions on the isolation system and on the piers for different bridge configurations subjected to both horizontal and vertical input, as a function of the characteristics of the model.
- To evaluate and quantify the effect of the axial force variations on the global response of the bridge, in order to investigate possible non-conservative approaches of the current design methods and to raise controversial issues deserving a more specific study.

3. Methods

The objectives of this research will be pursued using numerical approaches only. The analytical model will be tested using single pier models, on which static and dynamic parametric non-linear analyses will be performed. The factors influencing the axial force variation in the devices (such as deck aspect ratio, structural geometry and consideration of the vertical input) will be quantified. The structural system examined includes foundation, pier, isolation devices and deck section; all elements are modelled assuming a linear elastic response, with the exception of the isolators, represented by non-linear radial elements, whose response may be sensitive to axial force variations (AM model) or may not (NAM model).

The second objective stated above requires an exhaustive investigation of the most common deck cross sections. The fundamental geometrical parameter to classify the different cases has been identified in the deck aspect ratio $\beta = d/H$, where d is the distance between two vertical bearings (in our case the two FPS) and H is the vertical lever arm, equal to the distance between the centre of gravity of the deck mass and the FPS base. The expected axial force variation in the devices is directly related to β, as shown in Figs. 10 and 12.

Several different parameters have been considered to perform the parametric analyses required to evaluate the effects of considering axial force variation on the bridge response, such as the type of analysis, bridge configuration, number of spans, span length to pier height ratio, radius of curvature, deck aspect ratio, consideration of vertical input ground motion and the type of FPS analytical model. The assumed range of variation of these parameters will be justified and their influence on the results will be evaluated and discussed. The analytical model that will be adopted in this work concerns more properly the case of single pier bridges; the response of frame or wall-type piers is not considered in this step of the research.

The bridge response will be investigated in terms of displacement at the top of the piers, relative displacement between piers and isolators, shear demand at the isolation level and at the base of the pier, bending and torsional moment demand

on the piers. Clearly, the influence of adopting either one of the two FPS models will be carefully examined, to compare the variation of displacement and strength demand as a function of the FPS model and to evaluate the need of more complex modelling.

4. Friction Pendulum Analytical Model

A standard friction pendulum system (FPS) device is based on the principle of the sliding pendulum motion. It consists of two sliding plates, one of them (indifferently, the bottom or the top one) is characterised by a concave spherical surface. The two plates are connected by means of an articulated friction slider and PTFE bearing material, as schematically represented in the cross section depicted in Fig. 1(a). Typically a FPS device may provide equivalent dynamic periods of vibration in the range from 2 to 5 seconds and displacement capacities greater than 1 m. Detailed descriptions of the basic principles of the FPS devices can be found in literature in relatively recent works [Almazan *et al.*, 2002; Wang *et al.*, 1998; Tsai, 1997].

The FPS finite element idealisation adopted in the present research and described in detail in the following pages is shown in Fig. 1(b). In particular, the model developed in this study is characterised by a restoring force $\underline{V}$ and by a

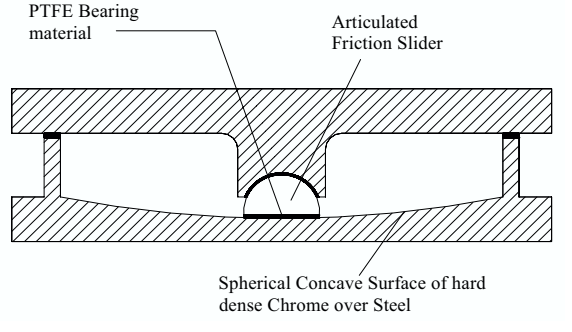

Fig. 1. (a) Radial section and (b) finite element representation of the FPS device (see also Fig. 2).

relative displacement $\Delta\underline{s}$ between the top and the bottom plates of the FPS (Figs. 2 and 3) where both $\underline{V}$ and $\Delta\underline{s}$ are radially-directed vectors, as discussed later.

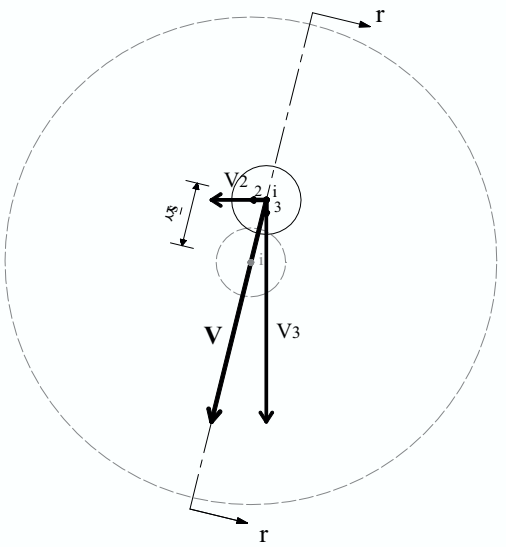

Fig. 2. Plan view (from the bottom) of a possible displacement of the articulated friction slider and description of the shear force components along the local axes 2 and 3 in the plane tangent to the spherical surface.

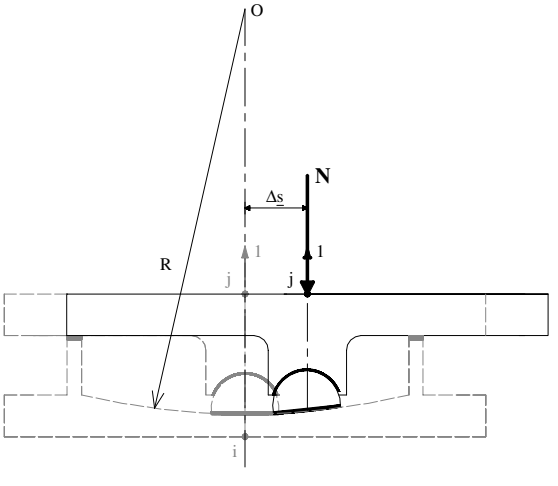

Fig. 3. Radial section $r - r$ (see Fig. 2) of the FPS model.

The behaviour of the isolator is described by the $\underline{V}$-$\Delta\underline{s}$ non-linear constitutive law and its main characteristic is to be sensitive to the axial load variations ΔN (AM model) (Figs. 4 and 5); for this reason the proposed model has a variable yield

point and a post-elastic stiffness that depend on the actual axial force, resulting in a non-linear post-elastic branch. It seems worth underlining that the majority of the models that can be found in literature depend on the initial axial load level, but they are usually insensitive to ΔN (NAM model), that is the post-elastic branch of the constitutive law remains linear.

In Fig. 4 the different features of the two models are shown; in particular the continuous lines are associated to the responses of the two isolators (AM model), one subjected to a progressive increase in compression and the other to a progressive decrease of axial load. On the opposite, if the NAM model is considered (dashed line), the response is insensitive to axial force variations.

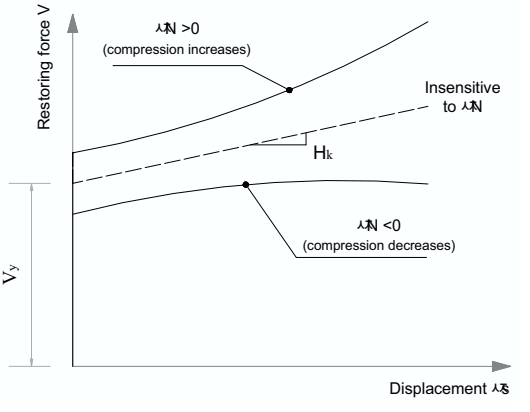

Fig. 4. Constitutive laws of FPS models sensitive (AM) and insensitive (NAM) to axial load variations.

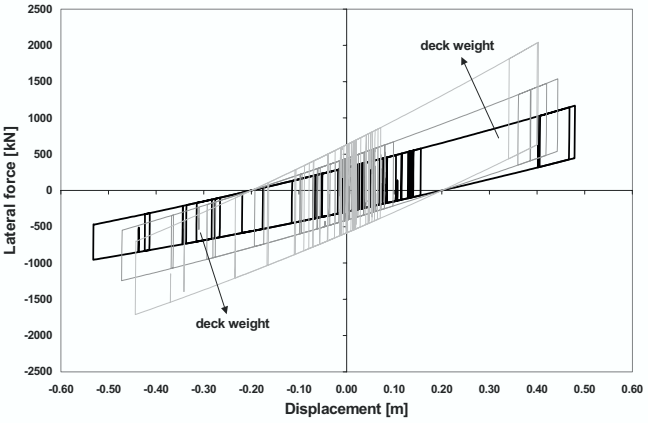

Fig. 5. Hysteretic loops of the model sensitive to the axial load variation (AM) for different initial axial forces.

The model of the isolator has been implemented by means of a 2-joint finite element [Fig. 1(b)]. The local axis 1 connects the joint i to the joint j; the two orthogonal local axes 2 and 3 lie in the plane perpendicular to the axis 1 and, for simplicity, they are always considered in this research oriented according to the transversal and the longitudinal directions of the bridge.

All the vectors used to describe the model lie in a plane tangent to the sliding surface which coincides with the local plane 2-3 (Figs. 2 and 3).

The fundamental equation describing the FPS radial shear V is the following:

$$\underline{V} = K_s \cdot (\Delta \underline{s} - \Delta \underline{s}_p)\,, \tag{1}$$

where:

$\underline{V}$ = radial shear of the FPS;
K_s = shear stiffness, constant value;
$\Delta \underline{s}$ = relative radial displacement;
$\Delta \underline{s}_p$ = relative radial plastic displacement.

The inelastic behaviour of the friction pendulum is described through the following equation:

$$\underline{F} = |\underline{V} - H_k \cdot \Delta \underline{s}_p| - V_y\,, \tag{2}$$

where:

H_k = post-elastic stiffness;
V_y = yielding shear.

The post-elastic stiffness and the yielding shear are assumed to be both functions of the axial load acting on the isolator, i.e. we set:

$$H_k = H_{k0} + c_h \cdot N\,, \tag{3}$$

$$V_y = V_{y0} + c_t \cdot N\,, \tag{4}$$

where:

H_{k0} = initial post-elastic slope;
V_{y0} = initial yielding shear;
c_h = curvature of the sliding surface ($= 1/R$);
c_t = coefficient of friction;
N = axial load on the isolator ($N > 0$, compression; $N < 0$, tension).

The temporal variation of the relative radial plastic displacement $\Delta \underline{s}_p$ is expressed by:

$$\Delta \dot{\underline{s}}_p = \dot{\gamma}\, \frac{\underline{V} - H_k \Delta \underline{s}_p}{|\underline{V} - H_k \Delta \underline{s}_p|}\,, \tag{5}$$

where:

$$\dot{\gamma} = 0 \quad \text{if } \underline{F} < 0 \quad \text{or} \quad \underline{F} = 0 \quad \text{and} \quad \dot{\underline{F}} < 0\,,$$

$$\dot{\gamma} > 0 \quad \text{if } \underline{F} = 0 \quad \text{and} \quad \dot{\underline{F}} \geq 0\,.$$

The resolution of the finite element problem of the FPS model is provided by means of time integration techniques. The fundamental quantities are computed through the integration of Eq. (5), assuming the solution at the time t_n is known and the relative radial displacement $\Delta\underline{s}$ in the time interval $[t_n, t]$:

$$\Delta\underline{s}_p - \Delta\underline{s}_p^n = \lambda \frac{\underline{V} - H_k \Delta\underline{s}_p}{|\underline{V} - H_k \Delta\underline{s}_p|}\,, \tag{6}$$

where:

$$\lambda = \gamma - \gamma^n\,.$$

The solution of Eq. (1) ÷ Eq. (5) in their discrete form is done with a "return map" algorithm [Simo and Hughes, 1998]. Assuming zero increment of the plastic sliding, a trial shear $\underline{V}^{\text{trial}}$ has to be firstly computed and used to derive $\underline{V}^{\text{cfr}}$ as follows:

$$\underline{V}^{\text{trial}} = \left\{ \begin{array}{c} V_2^{\text{trial}} \\ V_3^{\text{trial}} \end{array} \right\} = \left\{ \begin{array}{c} K_s \cdot (\Delta s_2 - \Delta s_{p,2}^n) \\ K_s \cdot (\Delta s_3 - \Delta s_{p,3}^n) \end{array} \right\} \tag{7}$$

$$\underline{V}^{\text{cfr}} = \left\{ \begin{array}{c} V_2^{\text{cfr}} \\ V_3^{\text{cfr}} \end{array} \right\} = \left\{ \begin{array}{c} V_2^{\text{trial}} - H_k \Delta s_{p,2}^n \\ V_3^{\text{trial}} - H_k \Delta s_{p,3}^n \end{array} \right\} \tag{8}$$

if the condition $\|\underline{V}^{\text{cfr}}\| \leq V_y$ is not satisfied, the sliding $\Delta\underline{s}_p$ is corrected by a factor λ, which is calculated by enforcing the yielding condition $\underline{F} = 0$ at the current time t. In particular expressing $\Delta\underline{s}_p$ as follows:

$$\Delta\underline{s}_p = \Delta\underline{s}_p^n + \lambda \frac{\underline{V}^{\text{cfr}}}{\|\underline{V}^{\text{cfr}}\|} = \Delta\underline{s}_p^n + \lambda \underline{N}^{\text{cfr}} \tag{9}$$

Equation $\underline{F} = 0$ can be written as:

$$|K_s(\Delta\underline{s} - (\Delta\underline{s}_p^n + \lambda\underline{N}^{\text{cfr}})) - H_k \cdot (\Delta\underline{s}_p^n + \lambda\underline{N}^{\text{cfr}})| = V_y\,. \tag{10}$$

Since the vectors of Eq. (10) are all parallel, it is possible to work only in term of modules instead of vectors to compute the unknown λ:

$$\lambda = \frac{\|\underline{V}^{\text{cfr}}\| - V_y}{K_s + H_k}\,. \tag{11}$$

The formulation of the tangent matrix required for the solution of the global problem using Newton algorithms is classically obtained from a consistent model linearisation [Simo and Hughes, 1998]. Details can be found in Ceresa [2002].

The proposed numerical model has been implemented in Feap, a computer code for static and dynamic non-linear analyses [Taylor, 2001]. Presently, the simulation

does not include possible uplift of the deck, therefore a tensile force in the isolator is permitted. This may result in an increase of compression on the other isolator on the top of the same pier and in an increased bending moment and shear. While this aspect may be easily taken into account in future studies, its relevance will be discussed whenever appropriate.

5. Seismic Input

The selection of the input ground motions to be used in this study was based on several requirements:

- the need of adopting natural records, in order to avoid possible bias related to abnormal frequency contents, number of cycle, duration and input energy;
- the necessity of a relatively high horizontal peak ground acceleration, to fully trigger the expected phenomena and to avoid large scaling that may affect the properties of the records;
- the importance of using a consistent set of two horizontal and one vertical components — more specifically the fundamental relevance of the vertical input is evident, since the focus of the study is on axial force variation effects;
- the wish of having a consistent, though relatively wide representation of magnitude, source mechanism, epicentral distance, duration, soil type.

On this basis, a set of five natural accelerograms (three components) was selected, as shown in Table 1.

All components of each one of them were scaled with a single factor, selected in such a way that the higher horizontal peak ground was set to 0.8 g. As a consequence, the pseudo-acceleration spectra of the horizontal components with the higher ground acceleration (plotted for a 5% damping in Fig. 6) are all showing the same level of acceleration for periods equal to zero, with significantly different amplification at different periods of vibration.

The difference between different ground motions is even more evident in Fig. 9, where the corresponding displacement spectra are depicted. Typical ratios of displacement demands at corresponding periods are in the order of four, with values typically ranging between 0.2 and 0.8 m.

In Figs. 7 and 8 the acceleration components in the second horizontal and vertical directions are depicted.

Given the fact that this study is not concentrating on seismic input issues, the set of ground motion is considered to be adequately representative.

6. Numerical Analyses

6.1. *Preliminary investigations on deck geometry and results on single pier models*

As previously pointed out, a rather extensive bibliographic investigation was carried out [Chen and Duan, 2000; L'industria Italiana del Cemento (IIC), 1996–2001;

Table 1. Properties of the natural original accelerograms (not scaled).

Earthquake	Record	Scale factor	Magnit. Mw	Arias intensity	Trifunac-Brady duration	PGA	PGV	PGD	Filter		Soil
									HP	LP	
				[m/s]	[s]	[g]	[cm/s]	[cm]	[Hz]	[Hz]	USGS
ChiChi, Taiwan 1999/09/20 TCU84	TCU84 V	0.692	7.6	2.342	18.70	0.340	25.3	11.94	0.09	50	B
	TCU84 N			3.898	25.10	0.417	45.6	21.27	0.10		
	TCU84 W			20.495	14.70	1.157	114.7	31.43	0.20	30	
Kobe 1995/01/16 KJMA	KJM up	0.974	6.9	1.88	10.40	0.343	38.3	10.29	0.50	null	B
	KJM000			8.475	9.94	0.821	81.3	17.68			
	KJM090			5.486	10.60	0.599	74.3	19.95			
Coalinga 1983/05/02 Pleasant Valley P.P. Yard 1162	HPVY UP	1.348	6.4	1.587	10.20	0.353	16.1	2.35	0.20	31	-
	HPVY 045			4.176	8.59	0.592	60.2	8.77		40	
	HPVY 135			3.883	10.30	0.551	36.4	3.96		31	
Northridge 1994/01/17 Newhall Fire Station	NWH-UP	1.356	6.7	2.897	7.46	0.548	31.5	16.27	0.12	23	C
	NWH-090			4.407	6.26	0.583	75.5	17.57			
	NWH-360			5.717	6.04	0.590	97.2	38.05			
Northridge 1994/01/17 Sylmar Converter Station East	SCE-UP	0.966	6.7	1.572	7.22	0.377	24.3	7.30	null	null	C
	SCE018			4.546	7.29	0.828	117.5	34.22			
	SCE288			2.928	7.84	0.493	74.6	28.69			

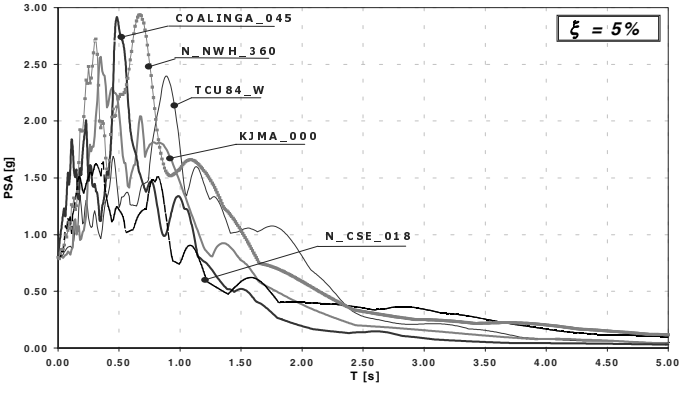

Fig. 6. Elastic pseudo-acceleration spectra scaled to 0.8 g (transversal component).

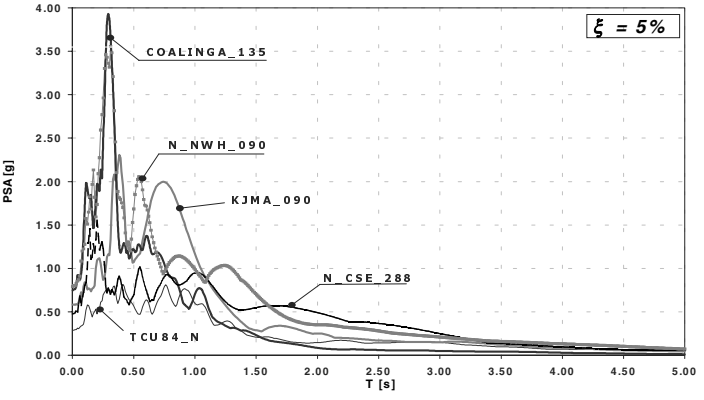

Fig. 7. Scaled elastic pseudo-acceleration spectra (longitudinal component).

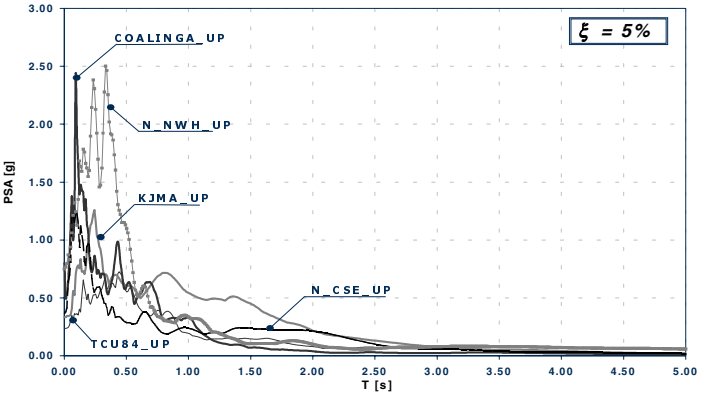

Fig. 8. Scaled elastic pseudo-acceleration spectra (vertical component).

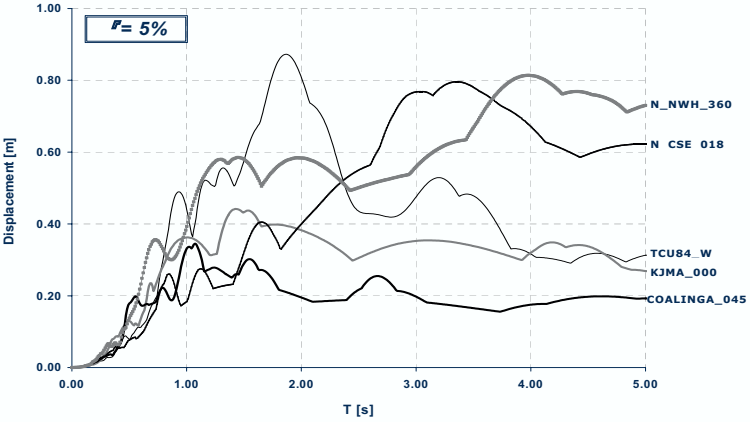

Fig. 9. Displacement spectra of transversal component scaled to 0.8 g.

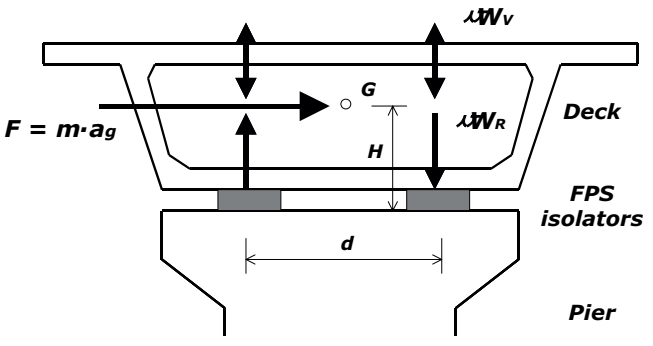

Fig. 10. Causes of the axial force variations on the isolators at the top of the pier.

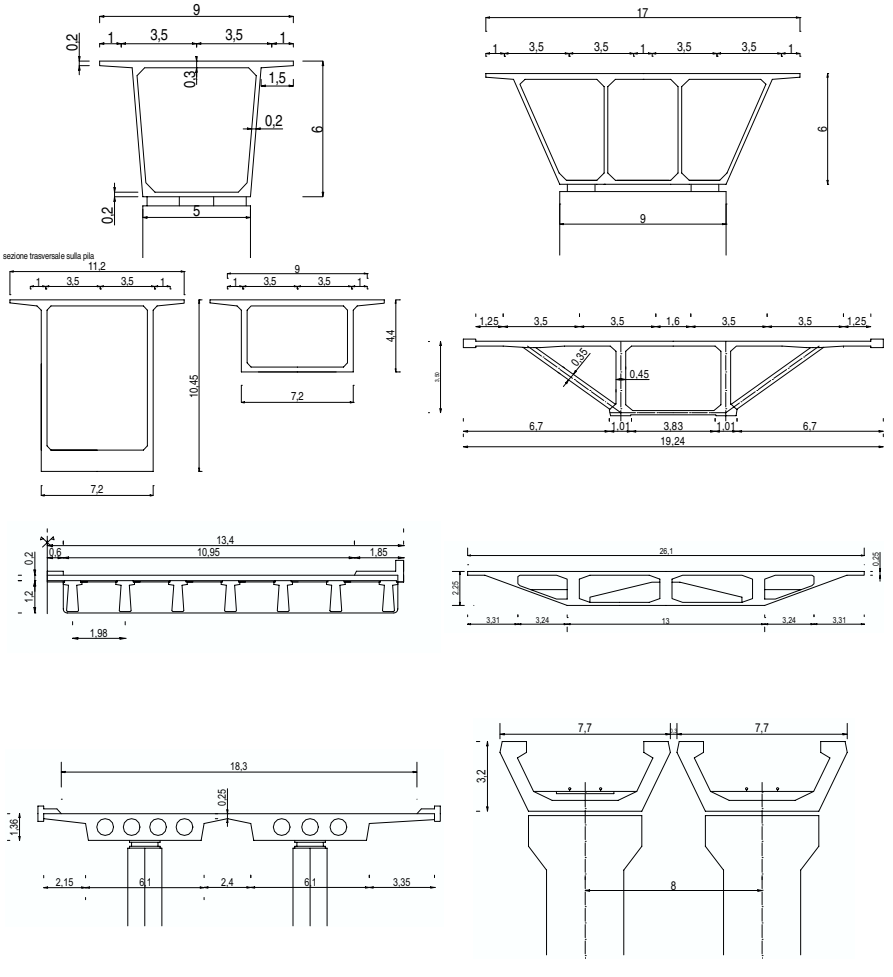

Fig. 11. Examples of existing deck cross sections.

Leonhardt, 1979; O'Connor, 1971] in order to identify the bridge deck cross sections most commonly used in the design practice. Some examples of common cases are depicted in Fig. 11, clearly showing that the aspect ratio may vary quite significantly. Within the scope of this study, the deck cross-section is characterised as a function of the geometrical parameter β, given by the ratio between the relative distance d of two bearings and the vertical distance H between the centre of gravity of the deck mass and the FPS base (Fig. 10).

This parameter controls the axial force variations ΔW_R due to the rotational equilibrium to lateral seismic load, characterised by opposite signs. A second axial force variation ΔW_V may be produced by the vertical component of the seismic input, this being characterised by the same sign on both bearings.

As shown in Fig. 4, an axial force variation results in a variation of the shear force transmitted by the bearing, and consequently in a different global shear at the pier top, in a possible torsional moment and in general in a different response under the earthquake motion. It has to be noted that the sum of the force variations on the two bearing may not be equal to zero even if the axial component of the input ground motion is neglected, depending on the plan geometry of the bridge.

Considering a static equilibrium and the horizontal component alone, to have a feeling of the relevance of the problem, the dimensionless axial force variation $\eta = \Delta W_R/W_o$ (where W_o is the initial gravity action) may be computed as a function of deck aspect ratio β and of the dimensionless horizontal acceleration $\alpha = a_g/g$ as:

$$\eta = \frac{\alpha}{\beta}\,. \tag{12}$$

This equation is graphically depicted in Fig. 12, together with the occurrence of section geometries found in the literature. It may be noted that β varies approximately between 1 and 10, with a concentration of cases between 1 and 3. While some care should be used in drawing general conclusion, because of the limited scope of the investigation, it is clear that axial force variation of the order of 30–40% may occur, even without taking into account the vertical component of the input ground motion.

On the basis of these results, the numerical simulations have been performed considering three values of β: 1.0, 2.5 and 5.0, the first value being typically representative of railway bridges, the second and third ones being more common for road bridges and viaducts. Considering that a limited axial force variation due to simple static equilibrium was expected for $\beta = 5$, this value was used only in case of curved configurations in plan where additional axial force variation may be produced by geometrical effect.

Preliminary numerical tests were performed on single pier models, of the type shown in Fig. 13: the mass distribution was representing the distributed mass along the pier stem and the concentrated masses at the pier head and at the deck centre of gravity. The FPS devices were modelled using either two AM and two NAM

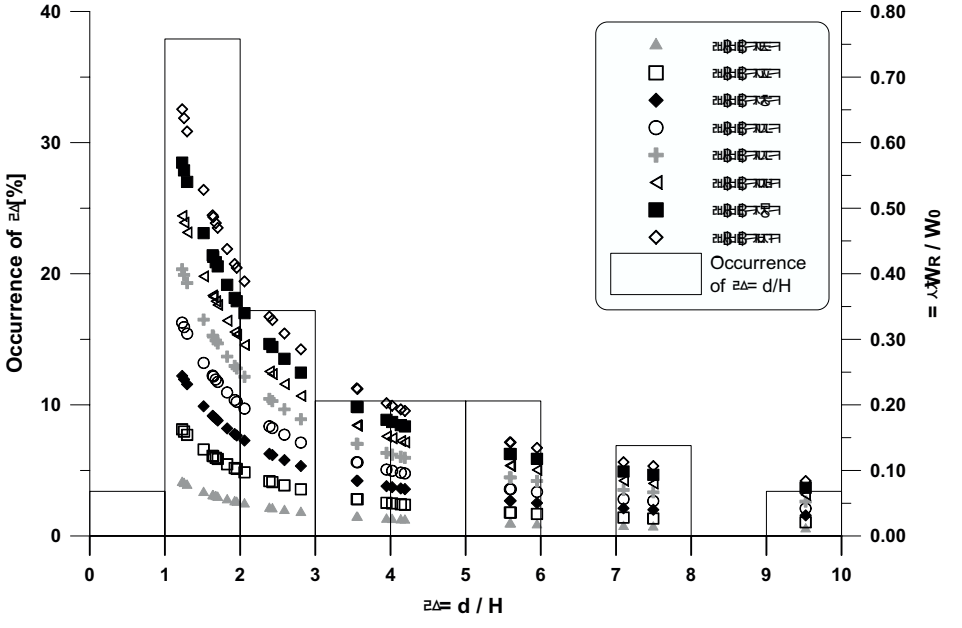

Fig. 12. Occurrences of β and axial load variations η as a function of β for different horizontal accelerations α.

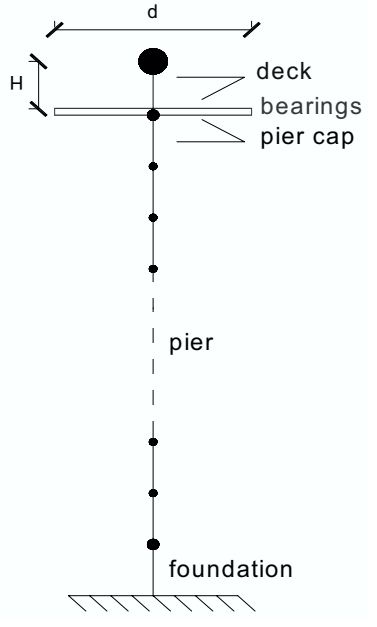

Fig. 13. Single pier model.

elements located at the appropriate distance (as a function of β). A friction coefficient c_t equal to 5% was adopted, together with a pendulum period of vibration equal to 4 seconds, from which the second stiffness of the model was determined as:

$$H_{k0} = \frac{W_o}{R} \quad \text{where} \quad R = \frac{T^2}{4 \cdot \pi^2} \cdot g \tag{13}$$

Quasi-static, pushover and time-history analyses were performed in order to examine the influence of different parameters (deck aspect ratio, pier height and deck mass) on the response, obtaining a confirmation of the following expected basic results.

- The maximum displacement demand on the pier-isolator system is substantially independent of the numerical model (AM or NAM).
- As expected and shown in Figs. 14 and 15, the response obtained using AM and NAM models differs significantly in terms of shear demand on each device, as a function of the axial load variation.
- The energy dissipated by the system does not depend on the model used, as a consequence of combination of axial force and shear variation with opposite sign on the two devices; this result should obviously be verified in the presence of deck curvature, irregularities in elevation and vertical component.
- The time histories analyses confirmed the trends shown in Fig. 12.
- The different shear actions in the longitudinal direction of the two AM elements may induce torsional demand, not captured by the NAM model (Fig. 14).

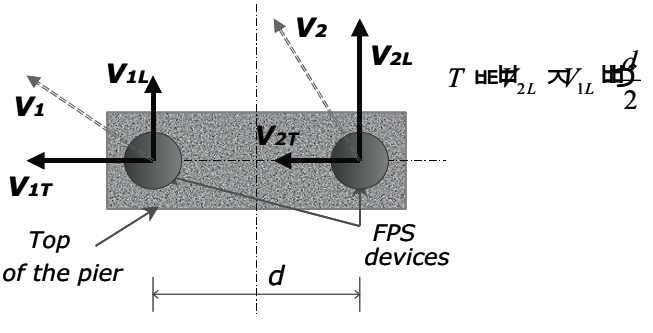

Fig. 14. Plan view: additional torsional action demand on the pier.

6.2. *Non-linear dynamic analyses on straight bridge models*

The straight bridge models consist of six piers of the same height, neglecting the effects of elevation irregularities.

The piers were modelled by frame elements fixed at the base, characterised by linear elastic behaviour and sections, depicted in Fig. 16, and considered cracked.

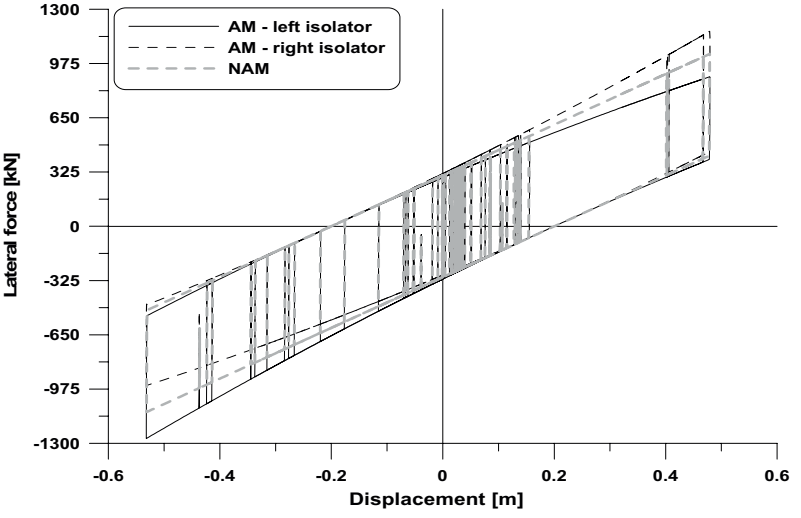

Fig. 15. Base shear — Top displacement diagram of a single pier model: Responses of the AM and NAM models.

Moment-curvature analyses were performed in order to calculate the flexural stiffness joining the origin to the yielding point, this one determined by an equal energy criterion (Table 2).

The deck was represented by linear elastic frame elements; the stiffness was kept constant (Table 2), without considering any effect of a variation of span length and aspect ratio.

Both AM and NAM models were considered to simulate the behaviour of the isolators at the top of the pier.

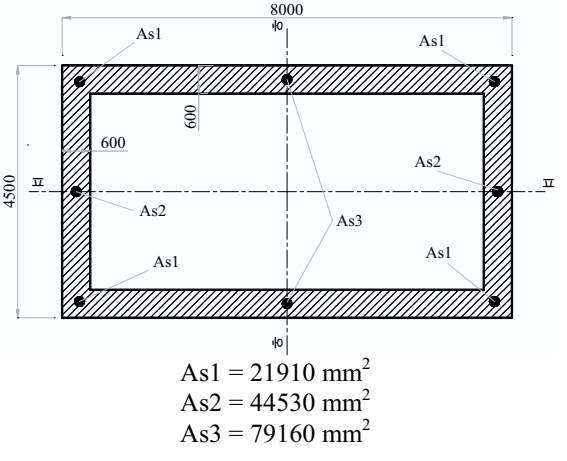

Fig. 16. Details of the pier section (dimensions in mm).

Table 2. Geometrical data for pier and deck sections.

	Pier	Deck
Area [m^2]	14.8	23
I_{33} [m^4]	39.1	7.9
I_{22} [m^4]	17.2	355.1

Table 3. Straight bridge configurations.

No. of piers	6
Span length [m]	15, 20, 25, 30, 39, 42, 60
$\beta = d/H$	1.00, 2.50
Pier height [m]	30
Accelerogram components	long. + transv., long. + transv. + vert.
FPS numerical models	Axial model (AM), Non Axial Model (NAM)

The five accelerograms described in Sec. 5 were used. A total of 280 analyses were performed, as resulting from the combination of the parameters shown in Table 3. No abutment was modelled, assuming that the model represents a section of a longer viaduct.

As a preliminary phase, cyclic quasi-static analyses were run applying an increasing deck displacement up to 0.60 m, both in the longitudinal and in the transversal direction, noting that significant effects become evident only in the second case, as reported in the following table.

Table 4. Cyclic quasi-static analyses: axial load variations imposing displacements in the longitudinal and in the transversal direction of the bridge; pier height = 30 m, $\beta = 2.50$.

Span length/Pier height	ΔW_{R_tot}[%]	$\Delta W_{R\_transv.}$[%]	$\Delta W_{R\_long.}$[%]
1	16	> 14	< 2
2	14	> 14	< 1

The time history analyses confirmed that bridge geometry, isolator model and consideration of vertical component do not affect displacement demand and dissipated energy, which remain essentially constant, with variations that never exceed 10%, as shown for some specific exemplificative cases in Figs. 17 and 18. As expected, the displacement demand is concentrated in the isolators, with negligible substructure displacements.

On the contrary, significant axial force variation may result on each device, as shown in Figs. 19 to 23, where the maximum values obtained in a single isolator during the response are depicted. These results have to be considered with some care, since a linear elastic model was used for the piers and no uplift was simulated (in several cases the variation shown is larger than 100%).

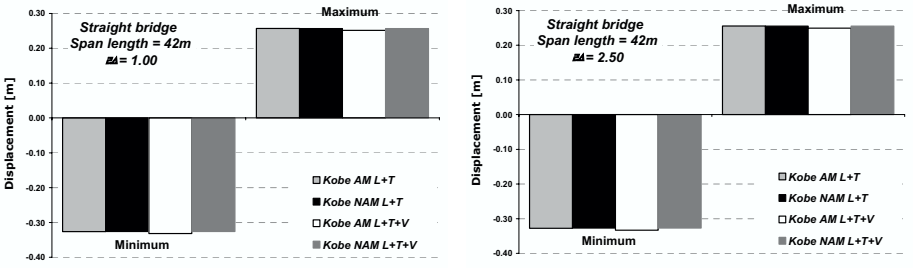

(a) (b)

Fig. 17. Maximum displacement demand comparisons, Kobe event; (a) aspect ratio equal to 1.00 and span length of 42 m; (b) aspect ratio equal to 2.50 and span length of 42 m.

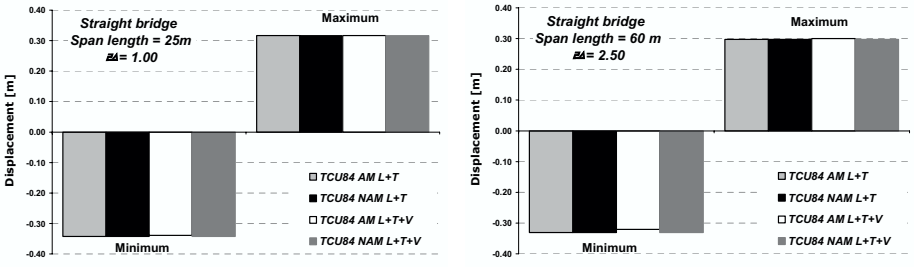

(a) (b)

Fig. 18. Maximum displacement demand comparisons, ChiChi event; (a) aspect ratio equal to 1.00 and span length of 25 m, (b) aspect ratio equal to 2.50 and span length of 60 m.

However, it may be noted that the presence of the vertical component is of the outmost importance, with negligible variations in case of responses to horizontal components only. The results are affected to a much lesser extent by a variation of the deck aspect ratio and by the model used (only in the case of the AM model this results in a different response though).

In Figs. 24 and 25 typical time histories of the axial force variation in time and typical force-displacement cycles of the isolator are shown, comparing the cases of 2 and 3 components input and of AM and NAM models.

Figure 25 confirms a result that is already pointed out, i.e. that the displacement demand is essentially the same in all cases. In absence of vertical input (Figs. 25(a) and 25(b)), similar displacements imply similar shear demand on the pier, as resulting from the combination of the contributions of the two devices, while in presence of vertical input [Figs. 25(c) and 25(d)] the axial force variation has the same sign on both isolators, possibly causing a significant increase of the total shear demand on the pier.

The peak values of the shear demand variation obtained using the AM model in presence of the three component of the input ground motion are reported in

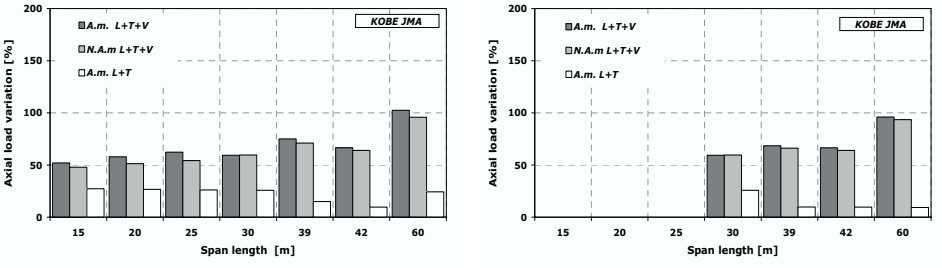

(a) (b)

Fig. 19. Kobe JMA, axial load variation with and without vertical input; (a) $\beta = 1.00$, (b) $\beta = 2.50$.

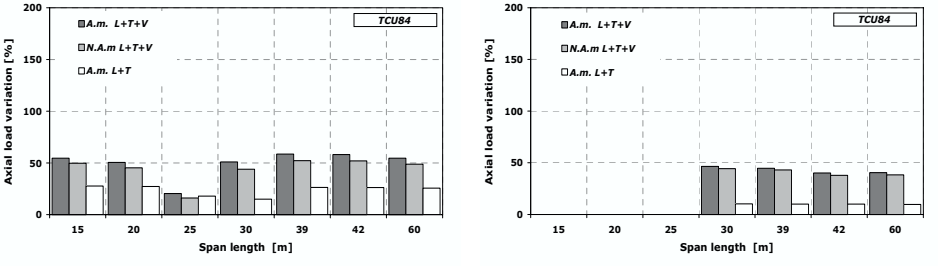

(a) (b)

Fig. 20. ChiChi TCU84, axial load variation with and without vertical input; (a) $\beta = 1.00$, (b) $\beta = 2.50$.

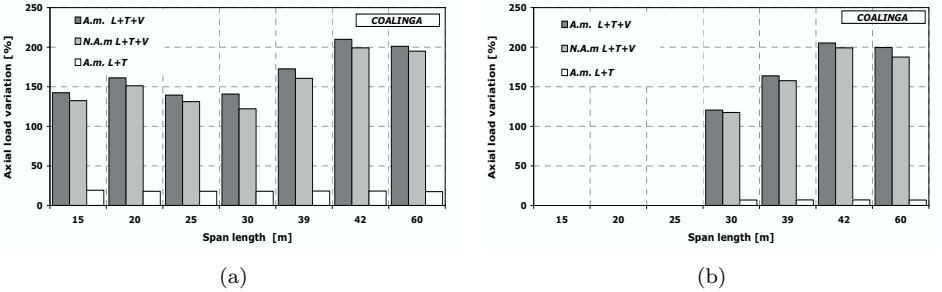

(a) (b)

Fig. 21. Coalinga, axial load variation with and without vertical input; (a) $\beta = 1.00$; (b) $\beta = 2.50$.

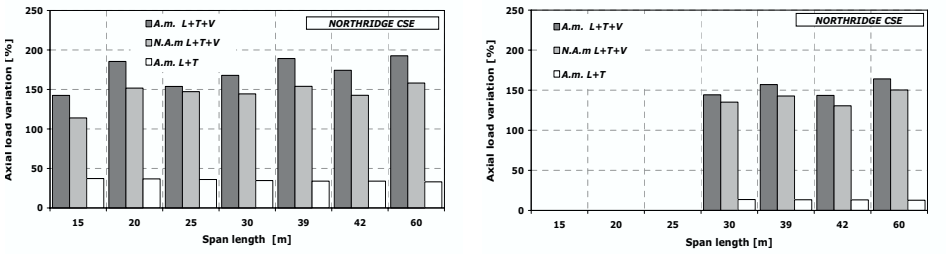

(a) (b)

Fig. 22. Northridge CSE, axial load variation with and without vertical input; (a) $\beta = 1.00$; (b) $\beta = 2.50$.

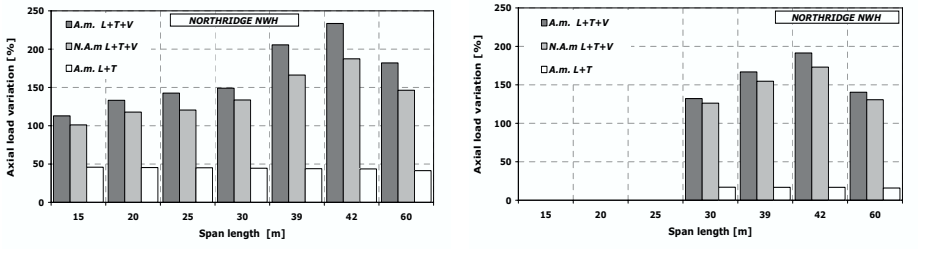

(a) (b)

Fig. 23. Northridge NWH, axial load variation with and without vertical input; (a) $\beta = 1.00$, (b) $\beta = 2.50$.

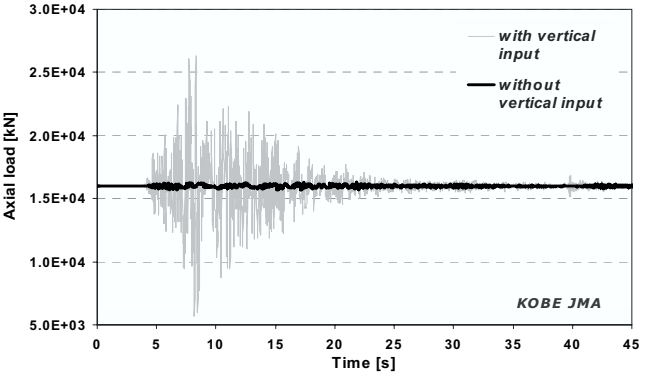

Fig. 24. Kobe JMA, axial load variation with and without vertical input, time history.

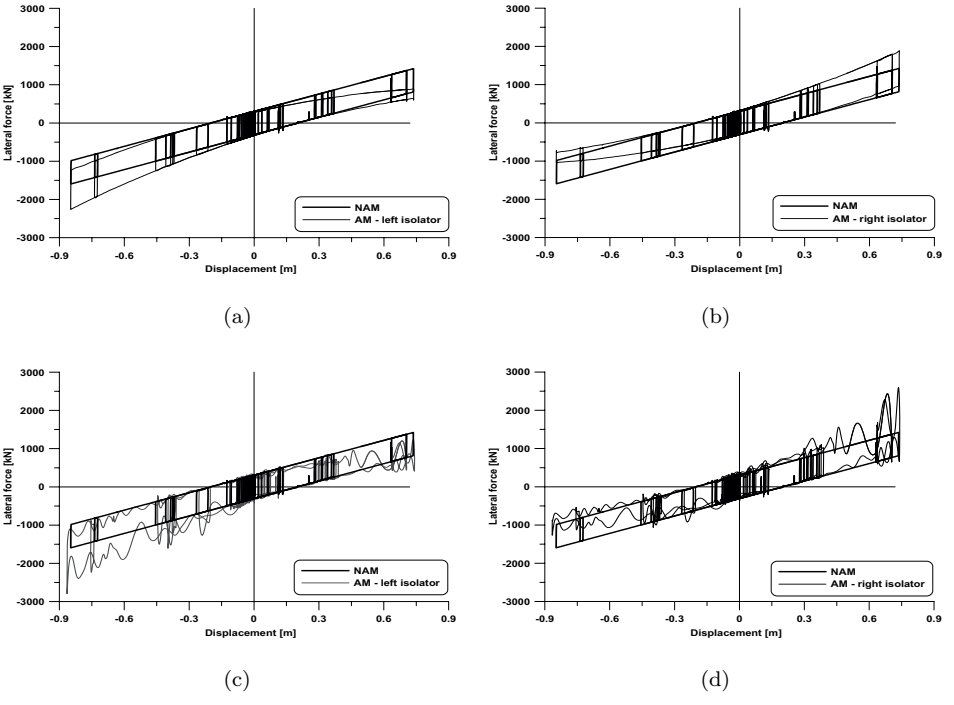

Fig. 25. Hysteretic loops of AM and NAM models, Sakaria event — (a) left isolator without vertical input, (b) right isolator without vertical input, (c) left isolator with vertical input and (d) right isolator with vertical input.

Figs. 26 to 30. Negligible variations (less than 5%, not shown in the figures) have been obtained neglecting the input vertical component, while when it is considered the effects may be of extreme relevance. All other parameters considered are of negligible importance when compared with the effects of different input ground motions.

Even when considering the Kobe and ChiChi events only (Figs. 26 and 27), where the response is not biased by possible uplifting effects, the shear demand

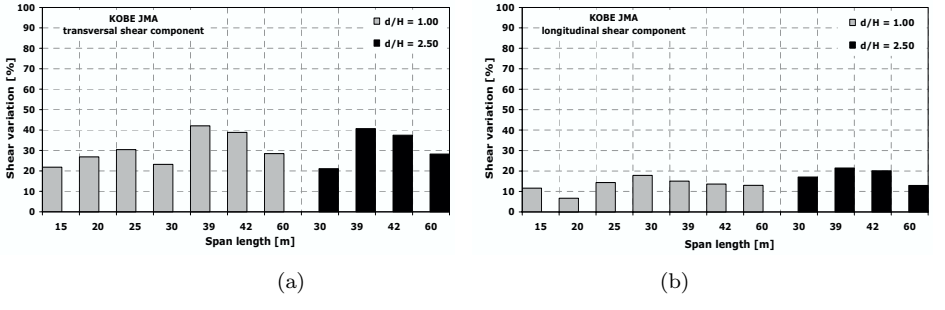

Fig. 26. Shear demand variation between the AM and the NAM models, Kobe earthquake; (a) transversal and (b) longitudinal component, vertical input considered.

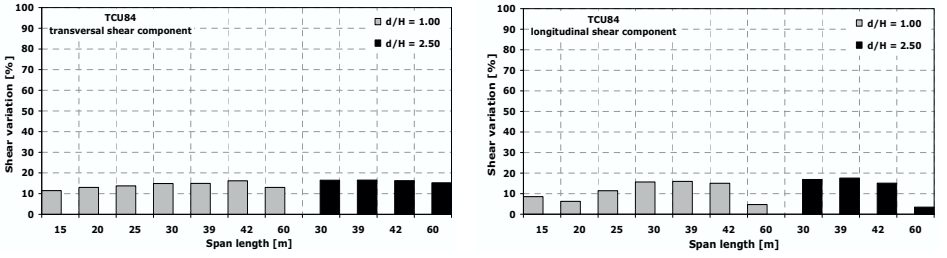

(a) (b)

Fig. 27. Shear demand variation between the AM and the NAM models, ChiChi earthquake; (a) transversal and (b) longitudinal component, vertical input considered.

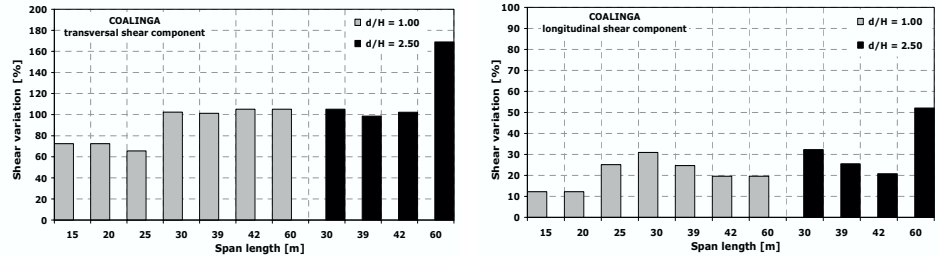

(a) (b)

Fig. 28. Shear demand variation between the AM and the NAM models, Coalinga earthquake; (a) transversal and (b) longitudinal component, vertical input considered.

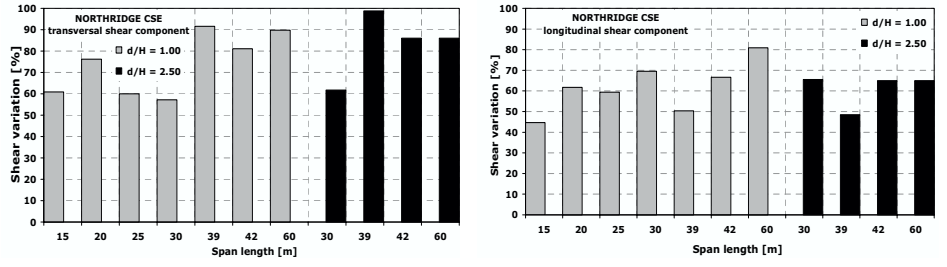

(a) (b)

Fig. 29. Shear demand variation between the AM and the NAM models, Northridge CSE earthquake; (a) transversal and (b) longitudinal component, vertical input considered.

in the transversal direction may increase by 42%, in the presence of relatively low peak vertical acceleration (ratio of vertical to horizontal peak acceleration equal to 0.30 and 0.41 in the two cases).

The average values of the maximum shear demand variations are shown in Fig. 31, being equal to 74% and 31% for the transversal and the longitudinal direction respectively. Considering the Kobe and ChiChi events only these values are

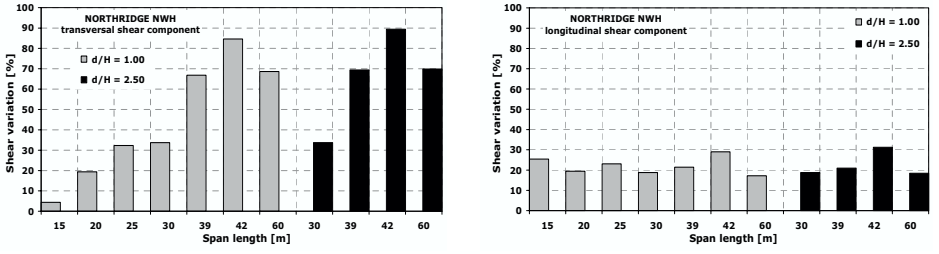

(a) (b)

Fig. 30. Shear demand variation between the AM and the NAM models, Northridge NWH earthquake; (a) transversal and (b) longitudinal component, vertical input considered.

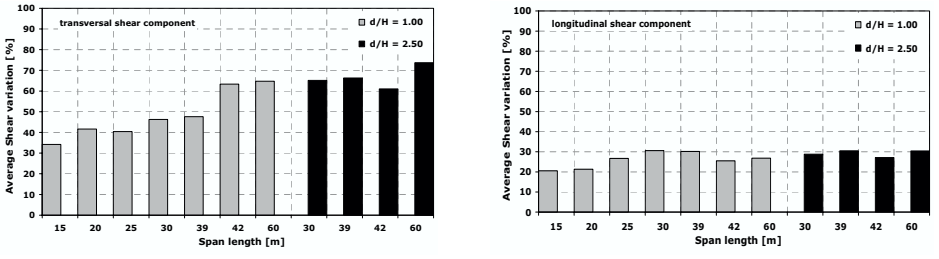

(a) (b)

Fig. 31. Shear variation between the two FPS models; (a) transversal and (b) longitudinal average values, vertical input considered.

(a) (b)

Fig. 32. Cases belonging to a given range of (a) transversal and (b) longitudinal shear variation between the two numerical models; vertical input considered.

reduced to 29% and 19%, being still significant. The number of cases obtained for peak shear variations below 20%, between 20 and 50% and greater than 50% are depicted in the pie plots of Fig. 32. It may be shown that for the cases of shear variation between 20 and 50%, certainly relevant for bridge design and assessment, no uplifting effect should be expected.

6.3. *Non-linear dynamic analyses on curved bridge models*

The seismic response of curved bridges isolated with FPS devices has been the subject of relatively limited studies in the past [Tsai and Huang, 1999]. Consistently

with the cases of straight bridges, the curved bridge models here investigated consist of six piers with the same height, constant span length of 30 m, variable in-plan curvature (with radius between 45 and 330 m, as given in Table 5) and piers oriented perpendicularly to local tangent of the deck curved axis. All the assumptions described for the straight-bridges cases still apply. The deck aspect ratio is now set to 5.00, therefore the expected axial force and shear variation will be essentially due to bridge geometry and vertical input.

The radius of curvature have been selected with reference to the limits recommended by the Italian standard [Ministero dei lavori pubblici, 2001] for highways, main roads and secondary extra-urban roads, as a function of road typology, design velocity and transversal slope.

Table 5. Curved bridge configurations.

No. of piers	6
Span length [m]	30
Radius of curvature [m]	45, 60, 75, 90, 120, 150, 180, 210, 240, 270, 300, 330
$\beta = d/H$	5.00
Pier height [m]	30
Accelerogram components	long. + transv., long. + transv. + vert.
FPS numerical models	Axial Model (AM), Non Axial Model (NAM)

Again, preliminary and pushover analyses were performed imposing an increasing horizontal displacement in the x and y directions (Fig. 33) up to a maximum value of 0.60 m. As expected, for curved bridges the axial force variations may be greater than those obtained for straight bridges, with a general trend to become negligible for increasing radius of curvature (Fig. 34). The time histories analyses confirmed the conservation of maximum displacement demand and dissipated energy, independently of FPS model, bridge geometry and presence of the vertical ground motion component, with differences lower than 10% (Fig. 35).

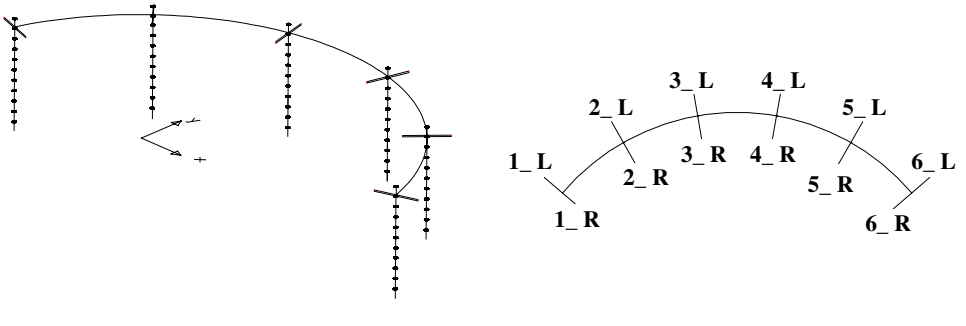

(a) (b)

Fig. 33. Curved bridge model: (a) Finite element mesh and mass distribution; (b) position of the FPS devices.

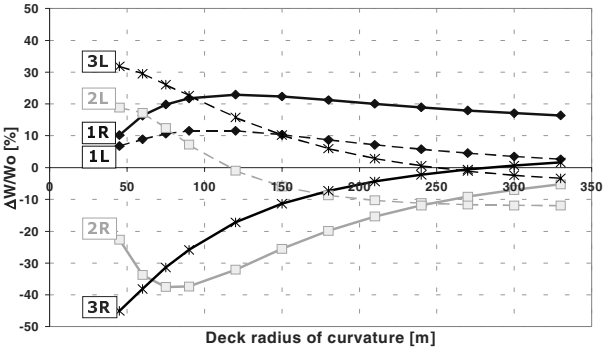

(a)

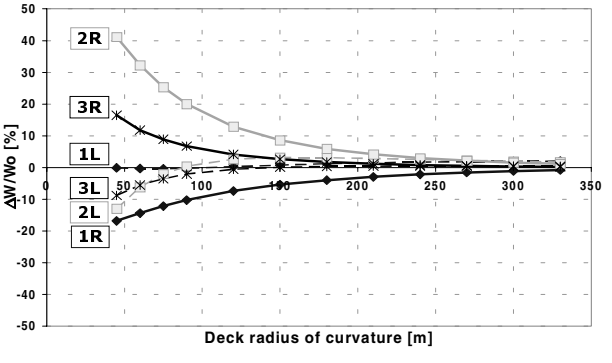

(b)

Fig. 34. Axial load variation as a function of the bridge radius of curvature, pushover analysis with imposed displacement along (a) the y and (b) the x axes.

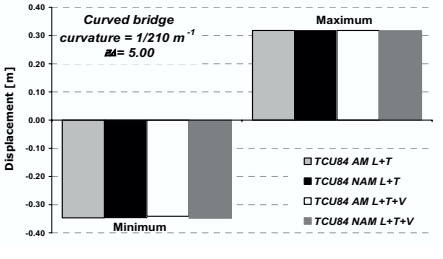

(a)

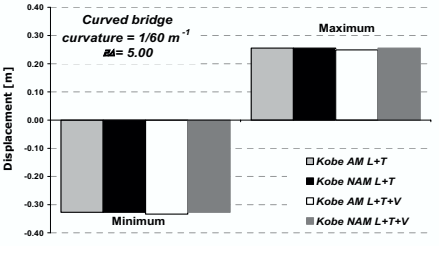

(b)

Fig. 35. Maximum displacement demand comparisons; (a) ChiChi event, radius of curvature = 210 m; (b) Kobe event, radius of curvature = 60 m.

The maximum axial load variations obtained from the time histories are shown in Figs. 36 to 38 for the different input ground motions, for the two bearing models

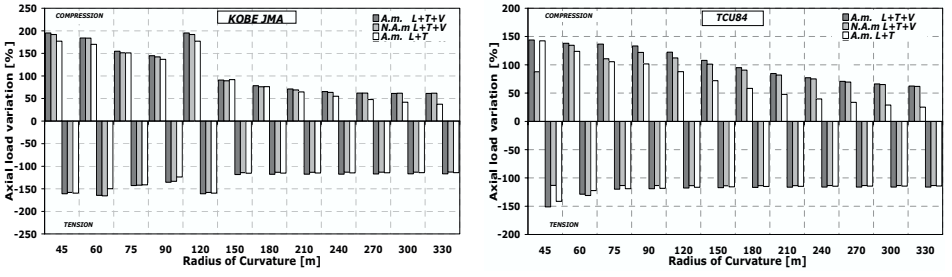

(a) (b)

Fig. 36. Peak values of the axial load variation as a function of the radius of curvature, the vertical input and the numerical model; (a) Kobe, (b) TCU84.

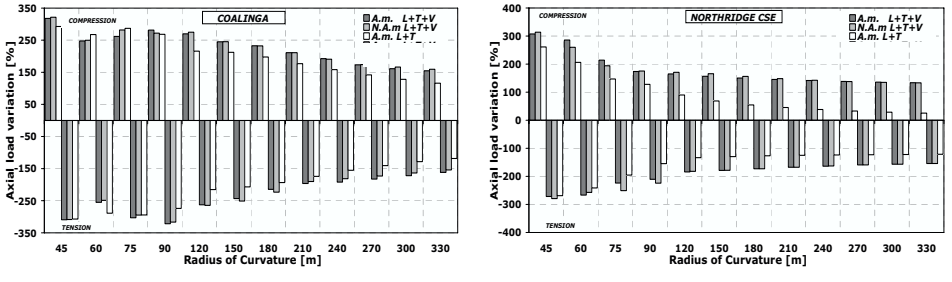

(a) (b)

Fig. 37. Peak values of the axial load variation as a function of the radius of curvature, the vertical input and the numerical model; (a) Coalinga, (b) Northridge Converter Station East.

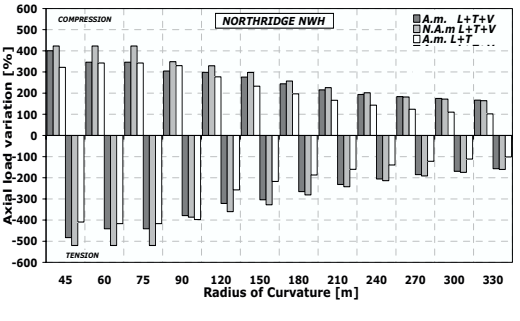

Fig. 38. Peak values of the axial load variation as a function of the radius of curvature, the vertical input and the numerical model; Northridge Newhall.

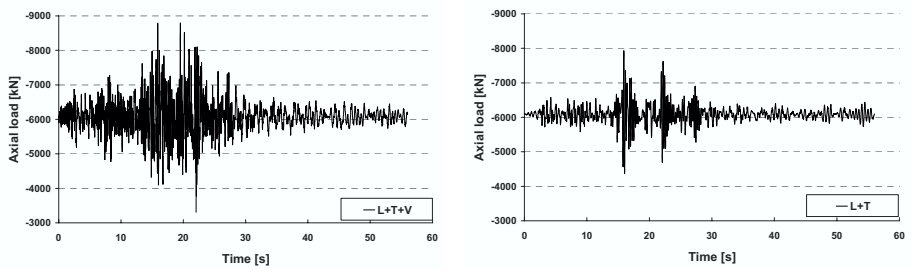

(a) (b)

Fig. 39. ChiChi TCU84, axial load variation (a) with and (b) without vertical input, time history.

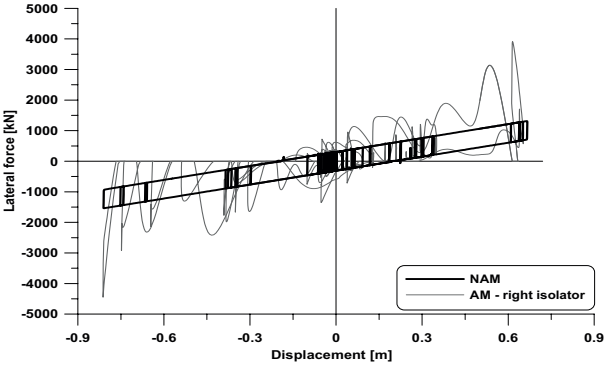

(a)

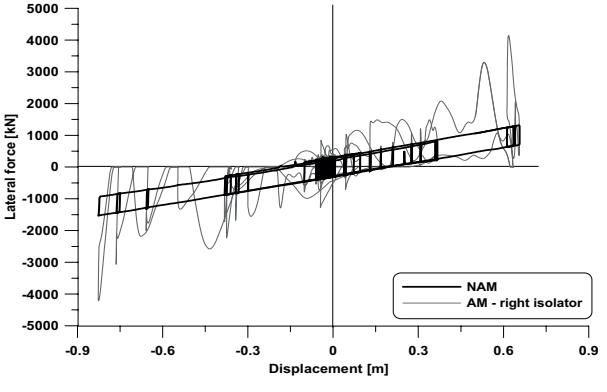

(b)

Fig. 40. Hysteretic loops considering and neglecting the effects of the axial force variations (a) without and (b) with vertical input, Sakaria event, pier #3, right isolator.

and including or excluding the vertical component. In general, the variations are significantly larger than in the case of straight bridges, with peak values, of the order of 150% for the ChiChi event, of 180% for the Kobe event, and much larger in all other cases. In all cases uplift has therefore to be expected, with the obvious tendency towards the results of the straight bridges for larger radius of curvature.

It has to be noted that the curved geometrical configuration implies significant axial force variation even neglecting the vertical component.

In Figs. 39 and 40 typical time histories of the axial force variation in time and typical force-displacement cycles of the isolator are shown, comparing the cases of 2 and 3 components input and of AM and NAM models; again, the relevance of including the vertical component is much more evident than in the case of straight bridges.

Displacement demand and dissipated energy are essentially independent of the numerical model, the geometry of the bridge, the application of the vertical ground motion (differences lower than 10%), while peak shear actions may differ significantly.

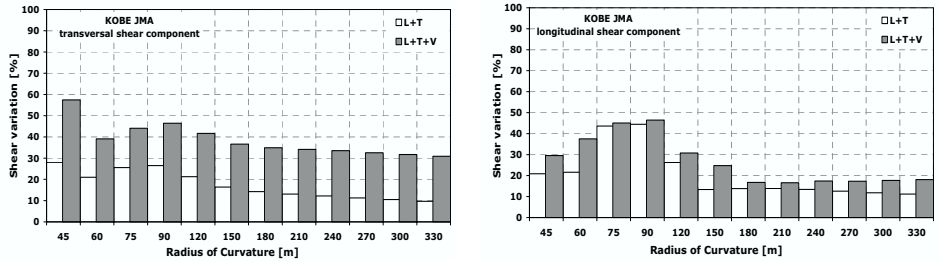

(a) (b)

Fig. 41. Shear demand variation between the AM and the NAM models, Kobe earthquake, (a) transversal and (b) longitudinal component.

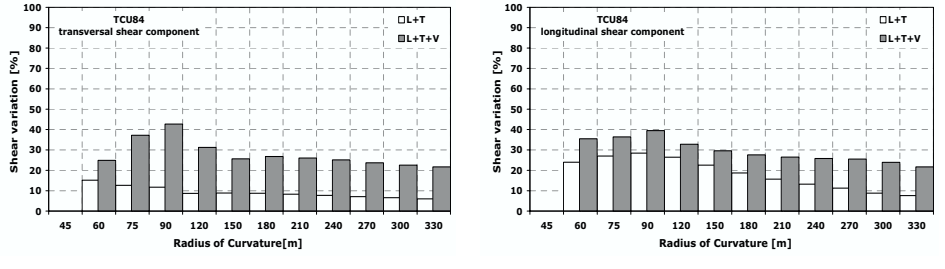

(a) (b)

Fig. 42. Shear demand variation between the AM and the NAM models, ChiChi earthquake, (a) transversal and (b) longitudinal component.

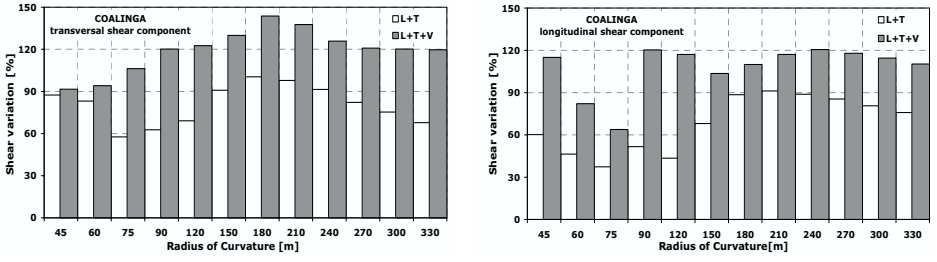

(a) (b)

Fig. 43. Shear demand variation between the AM and the NAM models, Coalinga earthquake, (a) transversal and (b) longitudinal component.

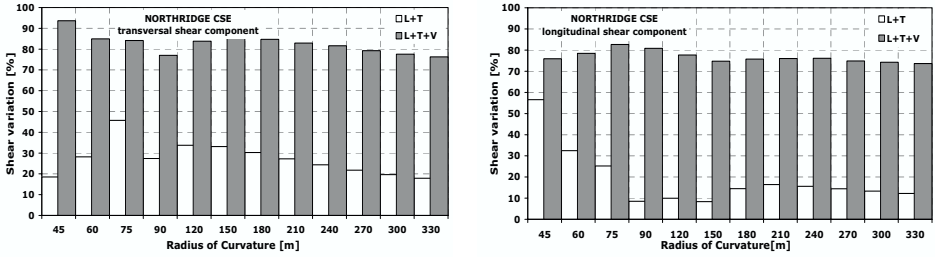

(a) (b)

Fig. 44. Shear demand variation between the AM and the NAM models, Northridge CSE earthquake, (a) transversal and (b) longitudinal component.

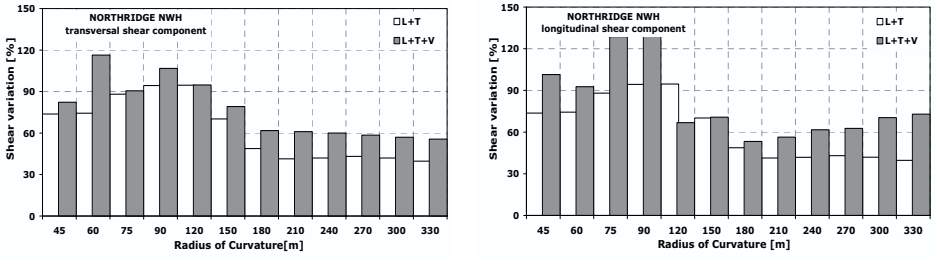

(a) (b)

Fig. 45. Shear demand variation between the AM and the NAM models, Northridge Newhall earthquake, (a) transversal and (b) longitudinal component.

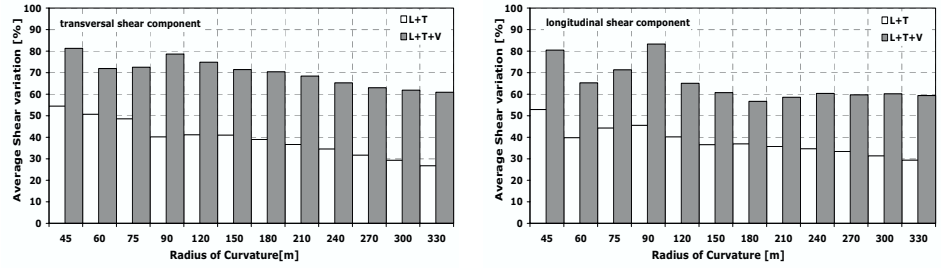

(a) (b)

Fig. 46. Shear variation between the two FPS models; (a) transversal and (b) longitudinal average values.

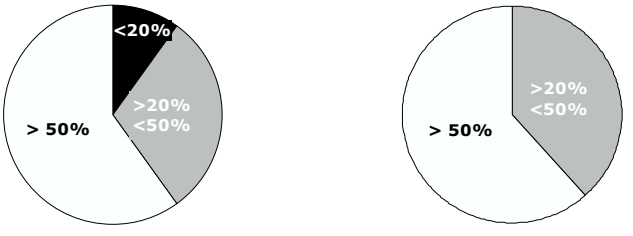

(a) (b)

Fig. 47. Cases belonging to a given range of (a) transversal and (b) longitudinal shear variation between the two numerical models; analyses with vertical input.

The maximum shear demand variations induced by the effects of axial force are plotted in Figs. 41 to 45 for all earthquake ground motions, showing the two directions components and the cases of including and excluding the vertical components; the average values of the maximum values obtained from all the dynamic analyses are shown in Figs. 46(a) and 46(b) and, finally, the number of cases obtained for peak shear variations below 20%, between 20 and 50% and greater than 50% are depicted in the pie plots of Fig. 47. Although the specific quantitative results may be biased by non modelled uplifting, the general trend is very clear, and the results obtained for straight bridges are emphasised.

7. Safety Verifications

In the previous sections, the potential importance of considering the effects of axial force variations on the seismic response of bridges isolated with friction pendulum systems was illustrated, showing that this may induce increased shear demands and possibly unpredicted torsional moment on the piers. To get a feeling of the possible relevance of these effects with respect to safety, it becomes necessary to consider capacity as well as demand and this obviously implies the need of designing sample

pier sections, and considering the actual variation of both demand and capacity as a function of axial force.

For this purpose, a specific sample case of a straight railway bridge was considered, characterised by six piers with a constant height of 10 m, span length of 39 m and deck aspect ratio equal to 1.00, designing longitudinal and transversal reinforcement according to standard code rules and design response spectrum (as defined in Eurocode 8 for stiff soil). Consistently with the input ground motions used for the non-linear analyses, a PGA equal to 0.8 g was assumed to anchor the spectra.

As a function of axial force level, bending, shear and torsional strengths of each pier were calculated at each time step of the time histories, using a standard flexural model for bending, a recently proposed model for shear [Kowalsky and Priestley, 2000], and a model proposed by Collins and Mitchell [1991] for torsion. The interaction between bending, shear and torsion [Collins and Lampert, 1971; Collins and Mitchell, 1991; Henry and Zia, 1982] was neglected, for simplicity, and anyhow consistently with the preliminary character of this part of the study.

The pier were designed assuming hollow rectangular sections with external dimensions equal to 3.20 m and 1.70 m and thickness of 0.35 m. The resulting percentages of the longitudinal and of the transversal reinforcement were $\rho_l = 3.15\%$ (1.7% if calculated on the gross area, neglecting the hole), $\rho_h = 0.23\%$ and 0.10% (inside and outside the critical region). The ratio of the pier mass to the supported deck mass was taken as equal to 15% and 30%.

The maximum variations of the shear demand at the top and at the base of the piers, obtained considering and neglecting axial force effects, are presented in Fig. 48 for three ground motions. It is evident that the presence of a relevant pier mass tends to reduce the effects noted at the pier top (peak values reached at different time steps). The same trend may be noted if the flexural demand is considered (Fig. 49). As already pointed out, these peak values may be of little relevance if they are not compared with the corresponding capacity, examining a time history response.

This kind of comparison is depicted in Figs. 50 to 53 for the Kobe and Northridge events. It appears that a shear failure outside the critical region should be predicted at several instants of some of the time histories, therefore confirming the potential relevance of the phenomenon.

In the case of Northridge CSE event, the curvature demand exceeds the capacity (in terms of yielding curvature) in both longitudinal and transversal directions (Table 6).

The displacement demands at the deck level and at the top of the pier are shown in Figs. 54 and 55. As expected, most of the displacement demand is taken by the isolation system, therefore justifying the assumption of linear response of the pier and confirming that no problem should arise in terms of flexural response.

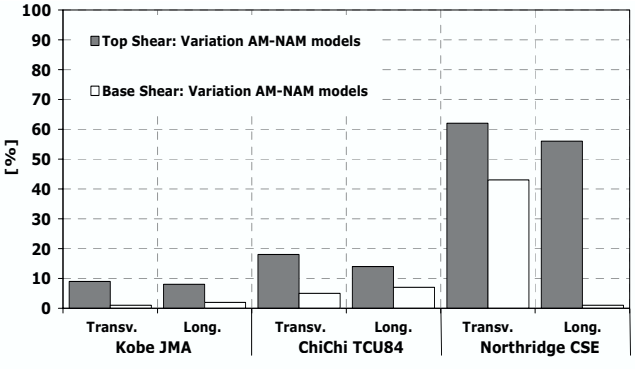

(a)

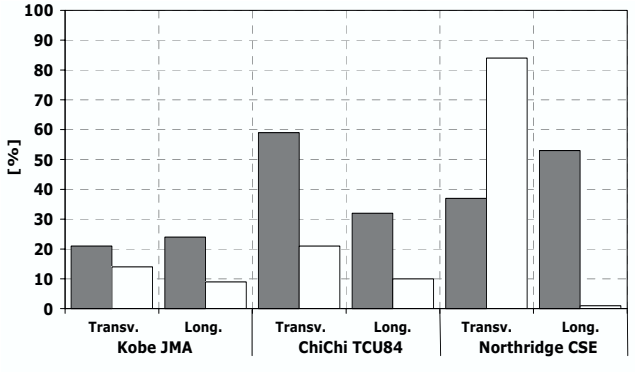

(b)

Fig. 48. Comparison between the responses in terms of variation of maximum shear demand at the top and at the base of the piers for pier mass/deck mass = (a) 30% and (b) 15%.

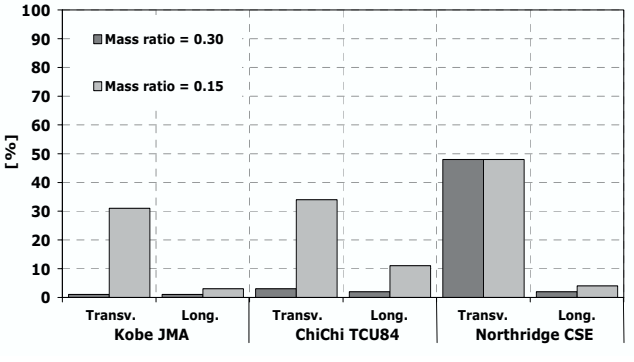

Fig. 49. Comparison between the responses in terms of variation of maximum bending moment demand at the base of the piers for pier mass/deck mass = 30% and 15%.

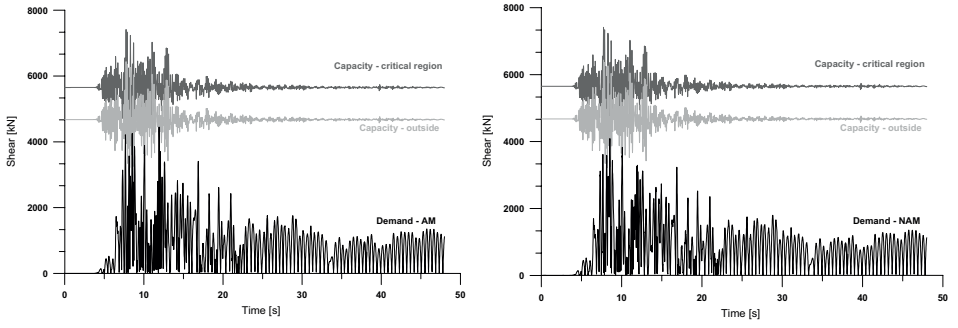

(a) (b)

Fig. 50. Base shear capacity–demand comparison along the longitudinal direction; (a) AM and (b) NAM demands, Kobe earthquake.

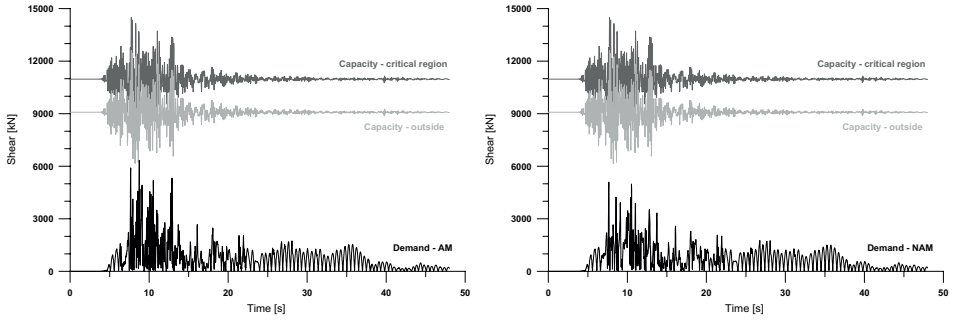

(a) (b)

Fig. 51. Base shear capacity–demand comparison along the transversal direction; (a) AM and (b) NAM demands, Kobe earthquake.

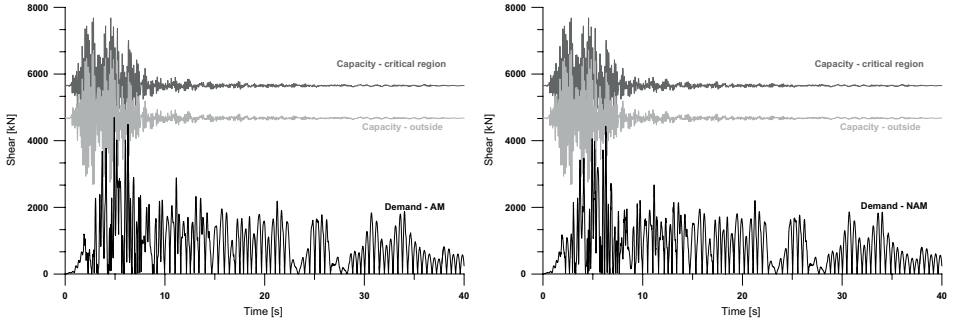

(a) (b)

Fig. 52. Base shear capacity–demand comparison along the longitudinal direction; (a) AM and (b) NAM demands, Northridge CSE earthquake.

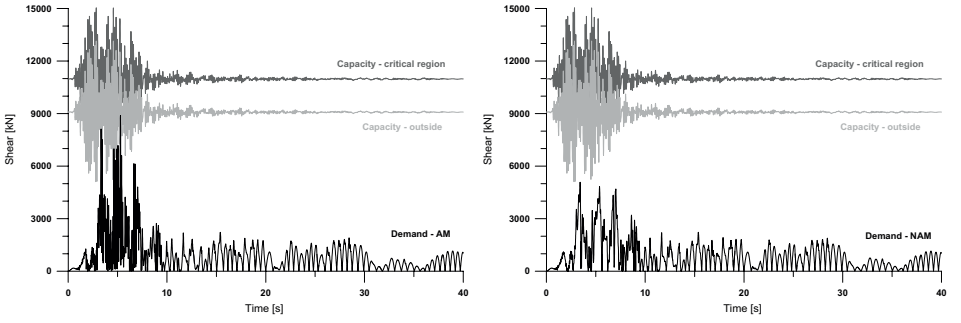

(a) (b)

Fig. 53. Base shear capacity–demand comparison along the transversal direction; (a) AM and (b) NAM demands, Northridge CSE earthquake.

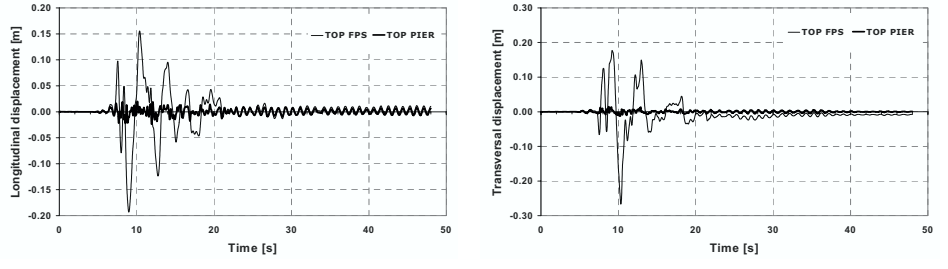

(a) (b)

Fig. 54. Global top displacement and pier displacement along (a) the longitudinal and (b) the transversal direction, Kobe earthquake.

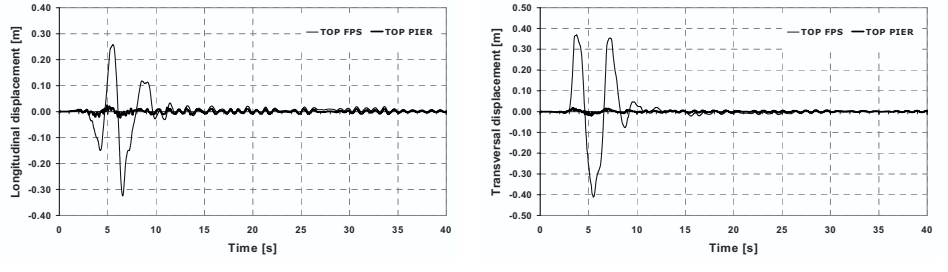

(a) (b)

Fig. 55. Global top displacement and pier displacement along (a) the longitudinal and (b) the transversal direction, Northridge CSE earthquake.

Table 6. Curvature capacity–demand comparison at the base of the piers, Northridge CSE earthquake.

Longitudinal direction					
		Curvature [m^{-1}] – Demand		Curvature [m^{-1}] – Capacity	
Time [s]	N [kN]	AM model	NAM model	yielding	ultimate
4.92	8940	3.297E − 03	2.796E − 03	3.157E − 03	1.560E − 02
Transversal direction					
		Curvature [m^{-1}] – Demand		Curvature [m^{-1}] – Capacity	
Time [s]	N [kN]	AM model	NAM model	yielding	ultimate
5.29	14 700	2.155E − 03	1.186E − 03	1.768E − 03	8.600E − 03

Finally, the maximum torsional demand resulting from the analysis is compared with the torsional capacity of the pier section considered in the analysis and with the capacity of a torsionally weaker section for different values of the axial force (Fig. 56). The torsional demand does not seem to be a problem in all cases considered, however, this aspect may deserve further attention, because of the interaction between shear and torsion.

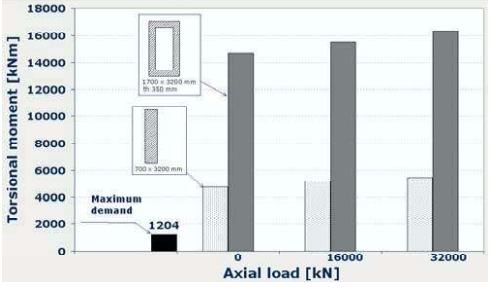

(a)

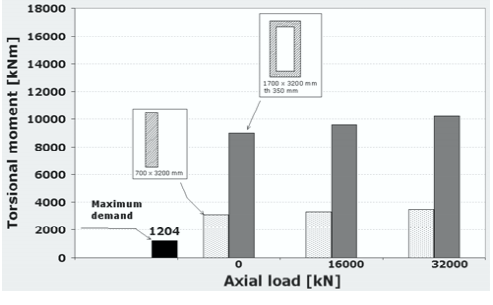

(b)

Fig. 56. Torsional demand compared with the capacity of different sections as a function of the axial load inside (a) and outside (b) the critical region. A hollow section of 1.70 m × 3.20 m and a rectangular thin section of 0.70 m × 3.20 m are considered.

8. Conclusions

In the research presented in this paper the effect of the axial force variations on the seismic response of bridges isolated with friction pendulum systems has been investigated. A series of parametric non-linear time history analyses have been performed using five ground motion records with the transversal components scaled to a maximum PGA of 0.8 g. The horizontal and vertical components of each seismic event have been considered. An analytical model of friction pendulum device whose yielding force and post-elastic stiffness are sensitive to the axial load variations has been developed.

The range of parameters considered has been rather ample, with the consequence that several potentially significant effects have been neglected. These include possible deck uplifting, bending–shear–torsion interaction, flexural non linear response of the pier.

Therefore, the conclusions of the study have to be considered as preliminary results to be further investigated in the future.

Generally speaking, the fundamental result is that the inclusion of axial force effects may not be significant for what concerns variation of the displacement demand, but may induce important increment of shear, bending and torsional moment demand on the piers. The fundamental parameters that may amplify, or reduce, these effects are the ratio between deck and pier mass, the aspect ratio of the deck, the radius of curvature of the bridge, the intensity of the ground motion and the consideration of vertical input, as briefly discussed below.

- Ratio between deck and pier mass: a significant variation of the shear force transmitted from the deck to the pier may result in strongly attenuated effect at the pier base when the ratio of the pier mass to the deck mass is high.
- Aspect ratio of the deck: for the same level of horizontal force, the axial force variation possibly induced by the horizontal acceleration is higher for a deck section relatively larger and for devices relatively closer one to each other.
- Radius of curvature of the viaduct: it is shown that a curved bridge may result in higher effects, due to the interaction of vertical and horizontal response.
- Intensity of the ground motion: relatively high horizontal peak ground accelerations may induce more significant effects, like in the case considered, where a PGA of 0.8 g is assumed.
- Consideration of vertical input: the inclusion of the vertical component of the input ground motion may result in being the crucial point to verify whether important effects have to be expected and considered.

These considerations may be of some help in deciding whether axial force effects may be neglected or should be considered in the analysis.

A fundamental aspect related to design concept should also be noted. Actually, when dealing with isolated bridges, it is common practice to assume that possible pier collapses are capacity protected by the shear capacity of the isolation system.

This implies that there is no reason to protect a possibly brittle shear collapse mode with a lower strength flexural yielding of the pier. Clearly, this situation may not apply if a significantly higher shear force is transmitted from the deck to the pier. As a consequence, it is felt appropriate to recommend that when using friction pendulum systems capacity design principles are still applied to protect undesired failure modes of the pier and foundation system.

A simple and immediate development of this work may consist of non-linear dynamic analyses with more refined models of the bridge elements (such as piers with non-linear behaviour), but also new parameters must be investigated (bridge configuration, irregularities in elevation, different deck types, framed piers, different isolator devices) in order to confirm the information obtained in this research.

Acknowledgements

The present research project has been founded by the European Community (SAFERR — Seismic Assessment for Earthquake Risk Reduction, HPRN-CT-1999-00035).

References

Almazan, J. L. and De La Llera, J. C. [2002] "Analytical model of structures with frictional pendulum isolators," *Earthquake Eng. Struct. Dyn.* **31**, 305–332.

Ambraseys, N. and Douglas J. [2000] "Reappraisal of the effect of vertical ground motions on response," *ESEE Report No. 00-4*, August 2000.

Ceresa, P. [2002] "Effetti di variazioni di azione assiale sulla risposta sismica di ponti isolati," *Degree Thesis*, Universitá degli Studi di Pavia.

Chen, W. F. and Duan, L. [2000] *Bridge Engineering*, Handbook (CRC Press).

Collins, M. P. and Lampert, P. [1971] *Designing for Torsion — Structural Concrete Symposium*, Toronto.

Collins, M. P. and Mitchell, D. [1991] *Prestressed Concrete Structures* (Prentice-Hall).

EC8 [1994] Eurocode 8 Design Provisions for Earthquake Resistence of Structures — Part 1-1: Seismic actions and general requirements of structures, ENV 1998-1-1; Part 2: Bridges, ENV 1998-2, Comite Europeen de Normalisation, Brussels.

Elnashai, A. S. and Papazoglou, A. J. [1997] "Procedure and spectra for analysis of RC structures subjected to strong vertical earthquake loads," *Journal of Earthquake Engineering* **1**(1), 121–155.

Ghobarah, A. and Elnashai, A. S. [1998] "Contribution of vertical ground motion to the damage of RC buildings," *Proceedings of the Eleventh European Conference on Earthquake Engineering*, Paris, France, ISBN 9054109823 (A. A. Balkema), September 9–13.

Henry, R. L. and Zia, P. [1982] "Prestressed beams in torsion, bending and shear," *Journal of the Structural Division, Proceedings of the American Society of Civil Engineers, ASCE* **100**, No. ST5.

Kowalsky, M. J. and Priestley, M. J. N. [2000] "Improved analytical model for shear strength of circular reinforced concrete columns in seismic regions," *ACI Structural Journal* **97**(3), 388–396.

Leonhardt, F. [1979] C.a. & C.a.p, I ponti (Edizioni tecniche), Volume VI.

L'industria Italiana del Cemento (IIC), *Associazione Italiana Tecnico Economica del Cemento (AITEC)*, *Roma*, Journal issues from 1996 to 2001.

Ministero dei lavori pubblici. Ispettorato generale per la circolazione e la sicurezza stradale, gennaio [2001] Norme funzionali e geometriche per la costruzione delle strade, Roma.

O'Connor, C. [1971] *Design of Bridge Superstructures* (John-Wiley & Sons, New York).

Simo, J. C. and Hughes, T. J. R. [1998] *Computational Inelasticity* (Springer-Verlag, New York), Chapter 1.

Taylor, R. L. [2001] "F.E.A.P. Manuals," Department of Civil and Environmental Engineering, University of California at Berkeley.

Tsai, C. S. [1997] "Finite element formulations for friction pendulum seismic isolation bearings," *International Journal For Numerical Methods In Engineering* **40**, 29–49.

Tsai, C. S. and Huang, C.-J. [1999] "Seismic behavior of isolated curved bridges with FPS isolators," *Proceedings of the Second World Conference on Structural Control*, John & Wiley, Chichester, England; New York **1**, 103–112.

Wang, Y.-P., Chung, L.-L. and Liao, W.-H. [1998] "Seismic response analysis of bridges isolated with friction pendulum bearings," *Earthquake Engng. Struct. Dyn.* **27**, 1069–1093.